

Precipitation Structure of Monsoon Rainfall Systems using S-band Vertically-Pointing Radar

Ultimate Chi-June Jung, Ben Jong-Dao Jou

Department of Atmospheric Sciences, National Taiwan University

Abstract

During early summer of 2013, the S-band vertically-pointing radar (VPR) was deployed with the Joss-Waldvogel disdrometer (JWD), optical disdrometers (Parsivel) and tipping-bucket rain gauge in National Taiwan University (NTU). The daily rainfall of each instruments showed good agreement and it provided us a good dataset to study the precipitation structure of monsoon rainfall systems. The collocated observations of a Mei-Yu front and a typhoon's rainband are shown to describe the evolution of reflectivity pattern and drop-size distribution. In the convective region, strong updraft and downdraft accompanying with heavy rainfall, and in the stratiform region, significant bright-band signature was found with much weaker vertical velocity. The strength of the bright-band and rain rate are in good agreement in the stratiform zone, i.e., the larger drops and stronger reflectivity associated with the bright band were found at the same time. Precipitation structures jointly observed by the VPR and disdrometers will provide opportunity to a better understanding of microphysical process associated with monsoon heavy rainfall systems.

Key word: vertically-pointing radar, drop-size distribution

1. Introduction

The S-band vertically-pointing radar (VPR) was introduced to Taiwan from May 2012 by Central Weather Bureau (CWB). The VPR has better vertical resolution (less than several hundred meters) than the operational radar network. It could help the researcher to get the details of precipitation system including the blank area below the lowest beam of surveillance radar.

Table 1. The operating characteristics of VPR.

Operating characteristics of VPR	
Mean frequency	3054 MHz
Peak power	30 kW
Vertical range	60-20400 m
Vertical resolution	60 m
Number of range gates	340
Averaging time	60 s
Beamwidth	3.3 degree
Pulse repetition frequency	2000 Hz

The VPR had been deployed in National Taiwan University (NTU), Taipei, Taiwan from January 2013. The pulsed Doppler radar is collocated with the Joss-Waldvogel disdrometer (JWD) and tipping-bucket rain gauge. The optical disdrometers (Parsivel) from Taiwan Typhoon and Flood Research Institute (TTFRI) were also deployed from April to June. It provided a good dataset to study the precipitation structure of monsoon rainfall systems.

The paper describes the rainfall data collected during 2013 and the VPR data quality in session 2. The observed results of a Mei-Yu front in May and a landing typhoon in July are described in session 3 and 4. Briefly conclusion is given in the last session.



Fig. 1. The instruments deployed in the NTU. From near to far: two Parsivel, two rain gauges (0.5 mm and 0.2 mm resolution), one JWD, and the VPR.

2. Data

The gauge in NTU has recorded more than 1000 mm of rainfall from February to July 2013. The precipitation system could be classified as winter time stable cold fronts (before May), relatively unstable Meiyu fronts (from May to June), afternoon thunderstorms and typhoons. The daily rainfall of different instruments deployed from April 19 to June 20 is shown below. Each instruments showed good agreement (Fig. 2).

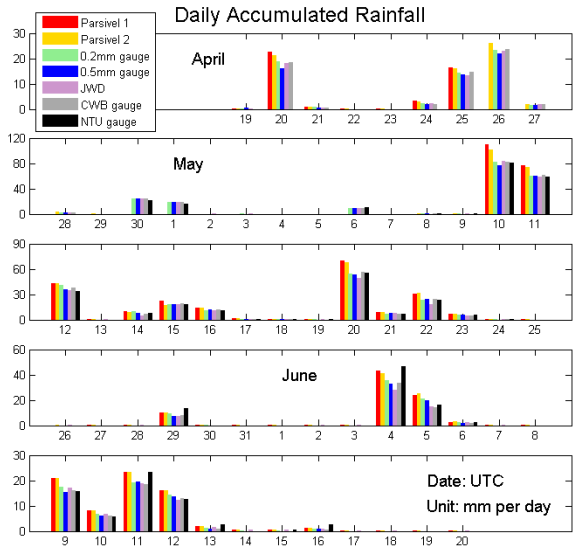


Fig. 2. Daily accumulated rainfall observed by the disdrometers and gauges (including CWB gauge site and NTU weather site). Different color represents the results from different instrument.

Table 2. The list of rain event. The gauge's accumulation is calculated using CWB gauge site data.

Event no.	Start time (UTC)		End time (UTC)		Gauge Rain total (mm)
	Date	Hour	Date	Hour	
1	2013/2/26	22:51	2013/2/27	08:25	24.5
2	2013/3/28	11:07	2013/3/28	18:29	16.0
3	2013/3/30	14:38	2013/3/31	04:35	17.5
4	2013/4/3	13:58	2013/4/3	22:50	14.0
5	2013/4/4	17:00	2013/4/4	19:46	11.0
6	2013/4/5	02:44	2013/4/5	16:59	14.5
7	2013/4/11	02:53	2013/4/12	02:43	58.5
8	2013/4/18	13:23	2013/4/19	00:50	16.5
9	2013/4/20	07:46	2013/4/20	21:46	14.5
10	2013/4/25	03:34	2013/4/25	11:49	13.5
11	2013/4/26	16:11	2013/4/27	01:38	25.5
12	2013/4/30	13:53	2013/4/30	23:08	24.5
13	2013/5/1	01:14	2013/5/1	08:41	18.0
14	2013/5/10	17:30	2013/5/11	18:46	144.0
15	2013/5/12	00:43	2013/5/12	18:22	36.5
16	2013/5/15	04:42	2013/5/15	09:00	19.0
17	2013/5/20	12:47	2013/5/21	00:34	47.5
18	2013/5/22	06:30	2013/5/22	09:30	22.0
19	2013/6/3	20:56	2013/6/4	05:46	29.0
20	2013/6/4	19:39	2013/6/5	04:08	18.0
21	2013/6/9	16:47	2013/6/9	19:20	16.0
22	2013/6/11	07:02	2013/6/11	12:16	18.0
23	2013/6/12	05:22	2013/6/12	10:35	13.0
24	2013/6/23	06:33	2013/6/23	07:53	40.5
25	2013/7/5	05:33	2013/7/5	10:09	42.5
26	2013/7/12	02:38	2013/7/13	08:52	85.5

The JWD measures the drop size distribution (DSD) by converting the impact of the falling hydrometeors to a drop diameter where the drops are assumed to fall at their terminal fall. The small drops are underestimated when two drops hit the sensor at the same time, known as dead time. This typically occurs at heavy rain. The JWD data was processed as following steps: remove tiny rainfall as noise and correct the under-measure small drops' number in heavy rain. In the presence of very large drops, the shortcoming of the under-measure small drops' number can lead to the underestimation of rain parameters, particularly reflectivity. Nevertheless, after the correction of JWD, the rain rates of JWD calculated using Gunn and Kinzer (1949) terminal velocity values are in good agreement with rain gauge (Fig 2).

Referring the method described by Tokay et al. (2009), after examining time series of rainfall measured by JWD, 26 rain events between February and July have been determined (Table 2). Events with total rainfall less than 10 mm have not been included. Consecutive rain events were separated based on the criteria there were at least two hours of rain-free conditions in between. Note that VPR failed during event 21. Several statistical methods have been applied to paired variables represented by reflectivity measured by different instrument. The statistics of the two variables (x and y) include the correlation coefficient ρ , the bias β , and the standard deviation of the difference (SD).

$$\rho = \frac{\text{Cov}(x, y)}{[\text{Var}(x)\text{Var}(y)]^{1/2}}$$

$$\beta = \frac{1}{n} \sum_{k=1}^n (x_k - y_k)$$

$$\text{SD}(x - y) = \sqrt{\text{Var}(x) + \text{Var}(y) - 2\text{Cov}(x, y)}$$

The authors investigate the time–height ambiguity between radar measurements aloft (4th gate) and JWD measurements at the surface. It has been studied by comparing the correlation coefficient, bias, and SD for the matched pairs of reflectivity (dBZ). The correlation between the JWD and Parsivel reflectivity was good (Fig.3a) but the reflectivity of Parsivel was about 1 to 2 dB higher than JWD's (Fig.3b). However, the rain rates of Parsivel are much higher than gauges and JWD, especially for higher rain rates. Lack of smaller drops in JWD and different terminal velocity measured by Parsivel are the possible reasons for the differences.

The correlation between the VPR and JWD is not as well as Parsivel and JWD (Fig 3a). It makes sense because the VPR sampling volume is hundreds of meters above the surface. The different condition of the rainfall path could lead to the lower correlation and higher SD.

All the events were merged for statistic excluded event 21-26 because of its bias are different from others. As Fig 4, the mean statistics of each height level were calculated by applying a weighting based on the sample size of each event. The 95% confidence intervals refers to the second lowest and second highest events when the event statistics were sorted from the lowest to the highest value. Since the absolute bias between paired radar and

JWD reflectivities exceeded 5 dB below the 4th gate, the measurements below this height was disregarded.

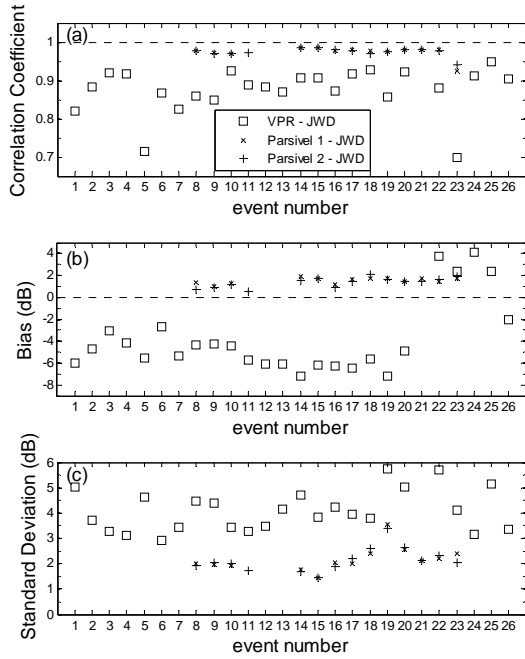


Fig. 3. Event-by-event comparison of reflectivity between VPR and JWD (\square); between Parsivel 1 and JWD, (\times); and between Parsivel 2 and JWD, ($+$). (a) The correlation coefficient, (b) bias, and (c) SD were presented to demonstrate the agreement between instruments.

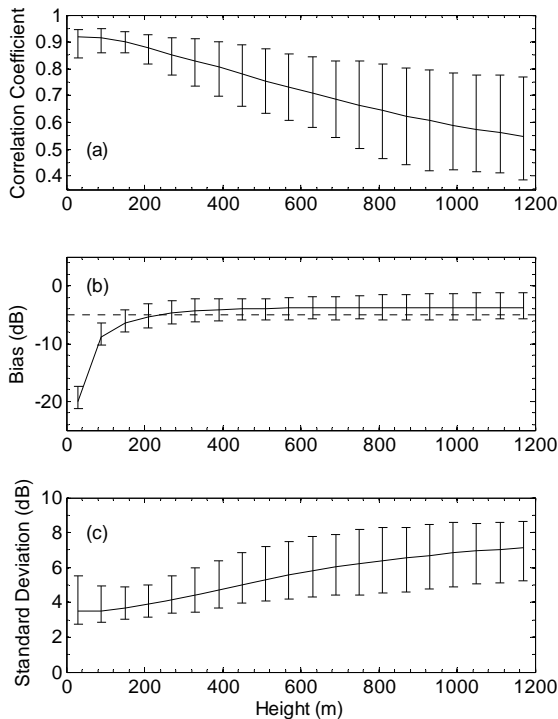


Fig. 4. Comparison of reflectivity between profiler and disdrometer (solid line) with height. The vertical bars represent the 95% confidence interval of the event-based (a) correlation coefficient, (b) bias, and (c) SD.

3. A Squall Line Case

From 19 May 2013, The Mei-Yu front slightly moved toward Taiwan then the frontal rainband propagated southeasterly through north Taiwan on 20 May producing heavy rainfall. The reflectivity map showed a significant convective line followed by broad weaker echo region, which was provided by the CWB Wu-Fen-Shan S-band surveillance radar 20 km far easterly from the NTU site. In the view of the rainband, the radial velocity showed the southwesterly wind in the front and the rear-to-front jet in the backside.

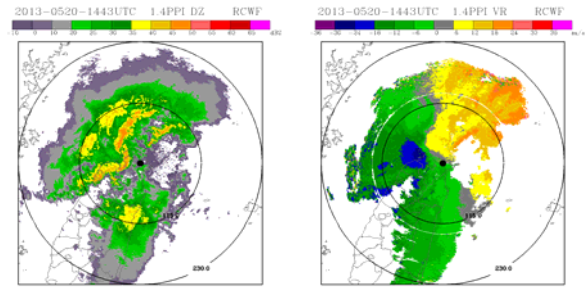


Fig. 5. Reflectivity (dBZ, left panel) and radial velocity (m s^{-1} , right panel) observed by Wu-Fen-Shan radar at 1.4 elevation angle of 1430 UTC 20 May 2013. The inner circle is 115 km radius from the radar and the outer one is 230 km radius. The VPR was 20km far westerly from the radar. This figure is provided by CWB.

This Mei-Yu frontal rainband is similar with the typical conceptual model of squall line; it could be divided into the convection zone, the transition zone, and the stratiform zone (Biggerstaff & Houze 1991). The VPR observation result is as Fig. 6. From 1430 to 1500 UTC, the stronger updraft (6 m s^{-1}) accompanying downdraft produced by rainfall could be identified. Also the 40 dBZ reflectivity region extended from surface to about 5 km high. The authors mark the period as convective region. From 1600 UTC till the precipitation end, the stratiform region with significant bright-band around 5 km high is identified. Between the convective and stratiform region, the reflectivity profile was not that consecutive. This hour is marked as the transition zone.

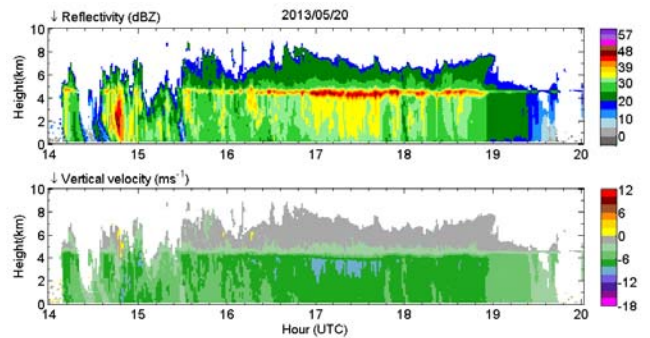


Fig. 6. Time-height diagram of reflectivity (dBZ, upper panel) and radial velocity (m s^{-1} , under panel) observed by VPR from 1400 to 2000 UTC 20 May 2013.

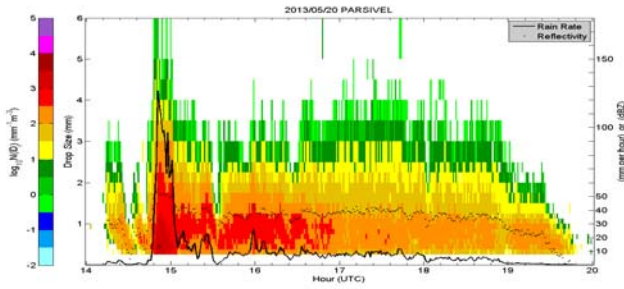


Fig. 7. Number density of raindrops observed by Parsivel from 1400 to 2000 UTC 20 May 2013. The black line represents the rain rate and the black dots represents the reflectivity calculated from the DSD.

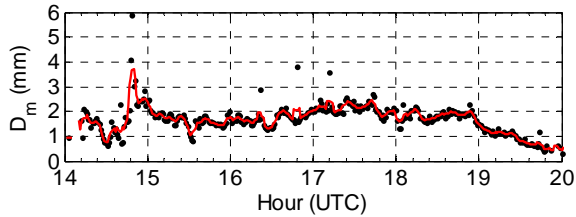


Fig. 8. Mass-weighted average diameter (D_m) calculated from the DSD observed by Parsivel. The black dot represents the D_0 every minute and the red line represents the 5-minutes moving average.

The past study (Biggerstaff & Houze 1991) showed that the iced particles in stratiform region are mainly transported backward from the convective updraft core. The strength of the bright-band and rain rate in the stratiform zone are gradually becoming stronger then weaker (Fig. 7). The Mass-weighted average diameter (D_m) is calculated,

$$D_m = \frac{\int_0^{\infty} N(D)D^4 dD}{\int_0^{\infty} N(D)D^3 dD} = \frac{M_4}{M_3}$$

Larger drops were identified at the same time of stronger bright-band occurred (Fig. 8).

The rain rate during transition zones was not very weak but even stronger than in stratiform zone. During this time, though the larger drops were less than in convective and stratiform region, but it produced more smaller drops than in stratiform region.

4. A Typhoon Case

Typhoon Soulik (2013) formed on the ocean north of Guam on 8 July 2013 then propagated WNW then NW toward Taiwan. The typhoon center positioned by CWB is shown as Fig. 9. The typhoon landed Taiwan around 1900 UTC 12 July accompanying with gust wind exceed 30 m s^{-1} then moved through south of Taipei City. It leads to the Wu-Fen-Shan radar temporary turned off to stand up to the strong wind. The weather radar of Taoyuan airport helped to monitor Soulik. The eye structure was clearly showed in the radar map (Fig. 10).

During its landing, the position of Soulik's center was near to VPR (see Fig. 9). So that there's good chance to observe inner core structure of typhoon using

VPR. The bright-band structure was significant around 5 km height before and after Soulik landed Taiwan (Fig. 11). It represents numerous iced / rimed particle embedded in the typhoon. The bright-band height became slightly higher while the typhoon approached the radar. It makes sense that the isotherm of 0 degree Celsius raised its height because of the typhoon's warm core structure.

Generally, the typhoon structure damaged after landing. The typhoon's eye is filled with cloud while the downward motion near the typhoon center decreased. Soulik's eye was clear just after its landing (Fig. 10), but the eye could not be identified while it passed through the south of Taipei City. The stronger updraft accompanying with higher reflectivity may even be found (Fig. 11).

The convective core is embedding in the strati form region. It could easily match the higher rain rate with the higher reflectivity (see Fig. 11 and Fig. 12). As Fig. 12 shows, the heavier rain occurred while the typhoon's center was on the ocean. Rain rate became smaller after typhoon landing. The raindrop size was mostly less than 3 mm equilibrium diameter (Fig. 12), and it consist with the past study of raindrop size of typhoon (Chang et al. 2009).

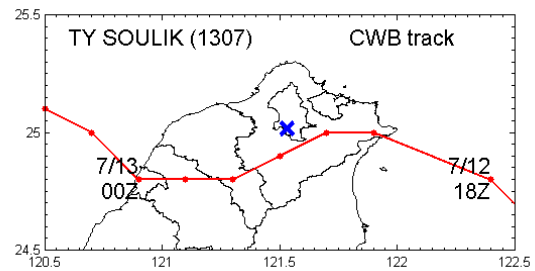


Fig. 9. Track of typhoon Soulik (2013) approaching and landing north Taiwan. The blue cross represents the location of VPR.

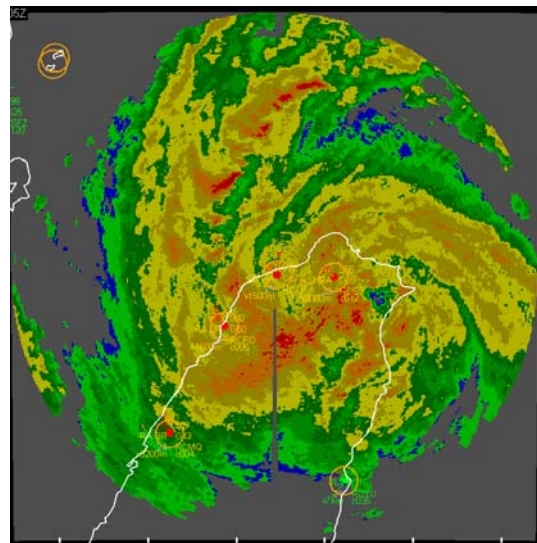


Fig. 10. Composite reflectivity observed by Taoyuan airport radar at 1905 UTC 12 July 2013. The figure is quoted from Civil Aviation Administration (CAA).

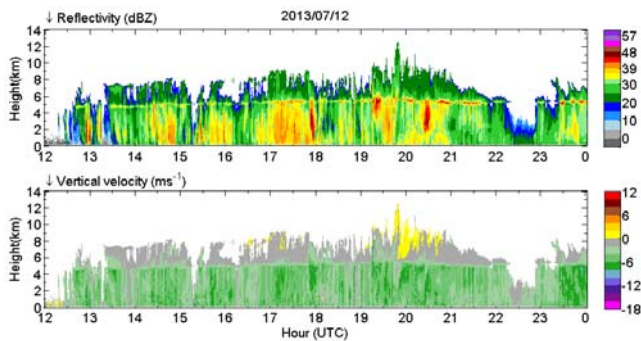


Fig. 11. Same as Fig. 6 except for 1200 to 2400 UTC 12 July 2013.

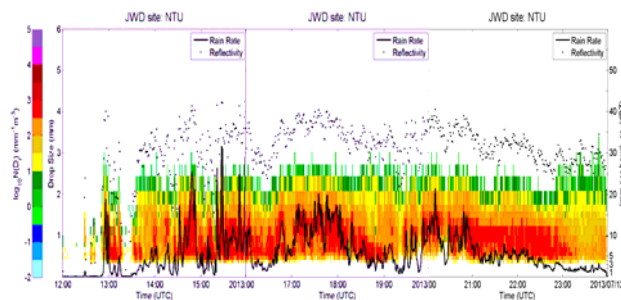


Fig. 12. Same as Fig. 7 except for 1200 to 2400 UTC 12 July 2013.

5. Summary

After the observation during spring and summer 2013, the authors get a dataset composed of VPR, disdrometer, and rain gauges. VPR data quality is checked first, then the data below the 4th gate (240 m height) was disregarded because of weaker reflectivity.

The collocated observation of a Mei-Yu front and a typhoon's rainband are showed to describe the evolution of reflectivity pattern and drop-size distribution. The authors could identify the convective region with stronger updraft accompanying downdraft via heavy rainfall, and the stratiform region with significant bright-band. The strength of the bright-band and rain rate in the stratiform zone was in good agreement. The larger drops were found at the same time of stronger bright-band occurred. The raised bright-band shows the typhoon's inner core approaching the VPR. The convective core in typhoon rainband is embedding in the stratiform region and the raindrop size of typhoon is seldom larger than 3 mm.

Precipitation structures jointly observed by the VPR and disdrometers will provide opportunity to a better understanding of microphysical process associated with monsoon heavy rainfall systems. More detailed analyses are ongoing.

The authors would like to thank Taiwan Typhoon and Flood Research Institute (TTFRI) supported the Parsivel. This study is funded by the National Science Council of Taiwan under Grant NSC102-2111-M-002-002 and by the Central Weather Bureau of Taiwan under Grant MOTC-CWB-102-M-10.

Reference

- Biggerstaff, M. I., and R. A. Houze, Jr., 1991: Kinematic and precipitation structure of the squall line. *Mon. Wea. Rev.*, **119**, 3034–3065.
- Bringi, V. N., V. Chandrasekar, J. Hubbert, E. Gorgucci, W. L. Randeu, and M. Schoenhuber, 2003: Raindrop size distribution in different climatic regimes from disdrometer and dual-polarized radar analysis. *J. Atmos. Sci.*, **60**, 354–365.
- Chang, W.-Y., T.-C. Chen Wang, and P.-L. Lin, 2009: Characteristics of the raindrop size distribution and drop shape relation in typhoon systems in the western Pacific from the 2D video disdrometer and NCU C-Band polarimetric radar. *J. Atmos. Oceanic Technol.*, **26**, 1973–1993.
- Fabry, F., and I. Zawadzki, 1995: Long-term radar observations of the melting layer of precipitation and their interpretation. *J. Atmos. Sci.*, **52**, 838–851.
- Gamache, J. F., and R. A. Houze, 1982: Mesoscale air motions associated with a tropical squall line. *Mon. Wea. Rev.*, **110**, 118–135.
- Gunn, R., and G. D. Kinzer, 1949: The terminal velocity of fall for water droplets in stagnant air. *J. Meteor.*, **6**, 243–248.
- Houze, R. A., 1993: *Cloud Dynamics*. Academic Press, San Diego, 573 pp.
- , 1997: Stratiform precipitation in regions of convection: A meteorological paradox?. *Bull. Amer. Meteor. Soc.*, **78**, 2179–2196.
- Sauvageot, H., and J.-P. Lacaux, 1995: The shape of averaged drop size distributions. *J. Atmos. Sci.*, **52**, 1070–1083.
- Sheppard, B. E., and P. I. Joe, 1994: Comparison of raindrop size distribution measurements by a Joss-Waldvogel disdrometer, a PMS 2DG spectrometer, and a POSS Doppler radar. *J. Atmos. Oceanic Technol.*, **11**, 874–887.
- Steiner, M., R. A. Houze, and S. E. Yuter, 1995: Climatological characterization of three-dimensional storm structure from operational radar and rain gauge data. *J. Appl. Meteor.*, **34**, 1978–2007.
- Tokay, A., and D. A. Short, 1996: Evidence from tropical raindrop spectra of the origin of rain from stratiform versus convective clouds. *J. Appl. Meteor.*, **35**, 355–371.
- , P. Hartmann, A. Battaglia, K. S. Gage, W. L. Clark, and C. R. Williams, 2009: A field study of reflectivity and Z–R relations using vertically pointing radars and disdrometers. *J. Atmos. Oceanic Technol.*, **26**, 1120–1134.
- Yuter, S. E., and R. A. Houze, 1995: Three-dimensional kinematic and microphysical evolution of Florida cumulonimbus. Part II: Frequency distributions of vertical velocity, reflectivity, and differential reflectivity. *Mon. Wea. Rev.*, **123**, 1941–1963.

